Nanoscale Horizons



COMMUNICATION

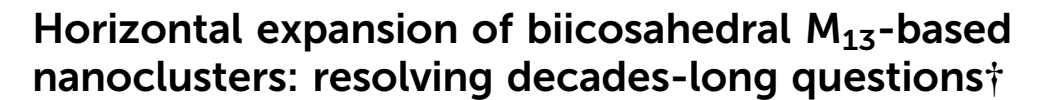
View Article Online



Cite this: Nanoscale Horiz., 2022, 7, 1397

Received 8th July 2022, Accepted 23rd September 2022

DOI: 10.1039/d2nh00321j rsc.li/nanoscale-horizons



Chuanjun Zhou, ‡ab Peiyao Pan, ‡ab Xiao Wei, ab Zidong Lin, Cheng Chen, Cheng Cheng Chen, Cheng Cheng Chen, Cheng Cheng Chen, Cheng Xi Kang * * and Manzhou Zhu * * * and Manzhou Zhu * * * and Manzhou Zhu * * and Manzhou Zhu * * and Manzhou Zhu * and Ma

For metal nanoclusters with the "cluster of clusters" intramolecular evolution pattern, most efforts have been made towards the vertical superposition of icosahedral nanobuilding blocks (e.g., from monoicosahedral Au₁₃ to bi-icosahedral Au₂₅ and tri-icosahedral Au₃₇), while the horizontal expansion of these rod-shaped multi-icosahedral aggregates was largely neglected. We herein report the horizontal expansion of the biicosahedral M25 cluster framework, yielding an [Au19Ag12(S-Adm)₆(DPPM)₆Cl₇]²⁺ nanocluster that contains an Au₁₃Ag₁₂ kernel and six Au₁(DPPM)₁(S-Adm)₁ peripheral wings. The structural determination of [Au₁₉Aq₁₂(S-Adm)₆(DPPM)₆Cl₇]²⁺ resolved a decades-long question towards rod-shaped multi-icosahedral aggregates: how to load bidentate phosphine and bulky thiol ligands onto the nanocluster framework? The structural comparison between [Au₁₉Ag₁₂(S-Adm)₆(DPPM)₆Cl₇|²⁺ and previously reported [Au₁₃Ag₁₂(PPh₃)₁₀Cl₈|²⁺ or $[Au_{13}Ag_{12}(SR)_5(PPh_3)_{10}Cl_2]^{2+}$ rationalized the unique packing of Au₁(DPPM)₁(S-Adm)₁ motif structures on the surface of the former nanocluster. Overall, this work presents the horizontal expansion of rod-shaped multi-icosahedral nanoclusters, which provides new insights into the preparation of novel icosahedron-based aggregates with both vertically and horizontally growing extensions.

1. Introduction

Metal nanoclusters have served as an emerging class of modular nanomaterials owing to their atomically precise structures

New concepts

The "cluster of clusters" evolution was one of the most fascinating features of intramolecular assembled nanoclusters. Hundreds of clusters have been constructed by systematically aggregating icosahedral M₁₃ nanobuilding blocks, and these rod-shaped aggregates were extensively studied owing to the strong electron coupling between substituent icosahedral units. However, most efforts were made towards the vertical superposition of icosahedral nanobuilding blocks (e.g., from monoicosahedral Au13 to bi-icosahedral Au25 and tri-icosahedral Au37), while the horizontal expansion of these rod-shaped multi-icosahedral aggregates was largely neglected. In this work, based on a newly developed M₃₁ nanocluster template, the horizontal expansion of the biicosahedral M25 dimer has been accomplished. The atomic-level structural determination of the Au₁₉Ag₁₂(S-Adm)₆(DPPM)₆Cl₇ cluster resolved two decades-long questions for rod-shaped multi-icosahedral aggregates, including (i) how to load bidentate phosphine ligands onto the nanocluster shoulder and (ii) how to arrange bulky thiol ligands onto the nanocluster waist. This work significantly broadens the research towards the "cluster of clusters" evolution pattern of metal nanoclusters.

and intriguing physical-chemical properties. 1-8 Besides, due to their programmably structure-dependent performances, metal nanoclusters or cluster-based hybrids have been customized for widespread applications such as catalysis, chemical sensors, drug delivery, biological imaging, and so on. 9-18 Typically, the structure of nanoclusters is composed of an internal metallic kernel and a peripheral ligand shell. 19-30 The structural determination of the metallic kernels of clusters at the atomic level has considerably inspired nanoscientists on a long-lasting question in nanoscience: what are the evolution modes from small-sized metallic complexes to nanoclusters or from nanoclusters to large-sized nanoparticles?^{1,31} Indeed, such a question has puzzled nanoscientists for decades because of two objective deficiencies of metal nanoparticles: the nonuniform molecule size and the uncertain surface environment.

With the continuous accumulation of the determined structures of metal nanoclusters, several intracluster evolution patterns have been observed experimentally, including cluster of

^a Department of Chemistry and Centre for Atomic Engineering of Advanced Materials, Anhui Province Key Laboratory of Chemistry for Inorganic/Organic Hybrid Functionalized Materials, Anhui University, Hefei 230601, P. R. China. E-mail: kangxi_chem@ahu.edu.cn, zmz@ahu.edu.cn

^b Key Laboratory of Structure and Functional Regulation of Hybrid Materials, Ministry of Education, Anhui University, Hefei 230601, P. R. China

^c Institutes of Physical Science and Information Technology, Anhui University, Hefei, Anhui 230601, P. R. China

[†] Electronic supplementary information (ESI) available. CCDC 2183917, 2163571, 2163572 and 2163804. For ESI and crystallographic data in CIF or other electronic format see DOI: https://doi.org/10.1039/d2nh00321i

[‡] These authors contributed equally to this work.

Communication Nanoscale Horizons

clusters, kernel fusion, interpenetration, shell-by-shell, layerby-layer, tetrahedron-based vertex-sharing, etc. 31 Among these patterns, the "cluster of clusters", which is first proposed in the 1980s, represents one of the most fascinating features of intramolecular assembled nanoclusters. 32-35 The icosahedral M₁₃ nanobuilding blocks can be aggregated by a vertexsharing mode (e.g., rod-shaped Au₂₅, Pt₂Ag₂₃, Au₃₇, Pt₃Ag₄₄, and Ag₆₁, ^{36–40} and pan-shaped Au₃₄Cu₃, Pt₃Ag₃₃, and Au₆₀), ^{41–43} a facesharing mode (e.g., Au₃₈ and Au₂₇Cd₁), 44,45 or an interpenetrating mode (e.g., Au₈Ag₅₅, Au₈Ag₅₇, and Au₁₅₆).^{46,47}

Among the cluster of clusters, rod-shaped aggregates of M₁₃ (M = Au/Ag/Cu/Pt/Pd/Ni) nanobuilding blocks have been extensively studied because of the strong electron coupling between substituent icosahedral units.31-35,40 However, most efforts were made towards the vertical superposition of icosahedral units (e.g., from mono-icosahedral Au₁₃ to bi-icosahedral Au₂₅ and tri-icosahedral Au₃₇), while the horizontal expansion of these rod-shaped multi-icosahedral aggregates is largely neglected.³¹ Besides, several questions remain unsolved regarding these nanoclusters. For example, for rod-shaped Au₂₅(PPh₃)₁₀(SR)₅Cl₂ with five monodentate PPh₃ at each shoulder and five thiol ligands at the waist,36 the outcome remains mysterious by substituting the monodentate PPh3 with bidentate phosphine ligands or regulating the SR as bulky thiol ligands in terms of two objective contradictions: (i) the oddnumbered coordination sites at the nanocluster shoulder (i.e., 5) versus the even-numbered coordination ability (i.e., 2n) of the bidentate phosphines, and (ii) the limited space at the nanocluster waist versus the large steric hindrance of bulky thiols. The problem solving towards such rod-shaped cluster models calls for more efforts.

Herein, the horizontal expansion of the rod-shaped biicosahedral M25 nanocluster was accomplished, yielding an [Au19Ag12(S-Adm₆(DPPM)₆Cl₇²⁺ nanocluster ($Au_{19}Ag_{12}$ for short; S-Adm = 1-adamantanethiol; DPPM = bis(diphenylphosphino)methane) that consists of a biicosahedral Au₁₃Ag₁₂ kernel, seven chlorine ligands, and six Au₁(DPPM)₁(S-Adm)₁ peripheral wings. Compared with the rod-shaped $[Au_{13}Ag_{12}(SR)_5(PPh_3)_{10}Cl_2]^{2+}$ $[Au_{13}Ag_{12}(PPh_3)_{10}Cl_8]^{2+}$ (Au₁₃Ag₁₂-S or Au₁₃Ag₁₂-Cl for short), the horizontal extension of unique Au₁(DPPM)₁(S-Adm)₁ surface units in Au₁₉Ag₁₂ was rationalized by the substitution of monodentate PPh3 with bidentate DPPM as well as the introduction of bulky S-Adm ligands. Control experiments were carried out to validate the decisive roles of both bidentate DPPM and bulky S-Adm in constructing the Au₁₉Ag₁₂ nanocluster. In this context, Au₁₉Ag₁₂ has served as a cluster model for resolving the abovementioned longstanding questions in rod-shaped nanoclusters with the "cluster of clusters" intramolecular evolution pattern.

2. Results and discussion

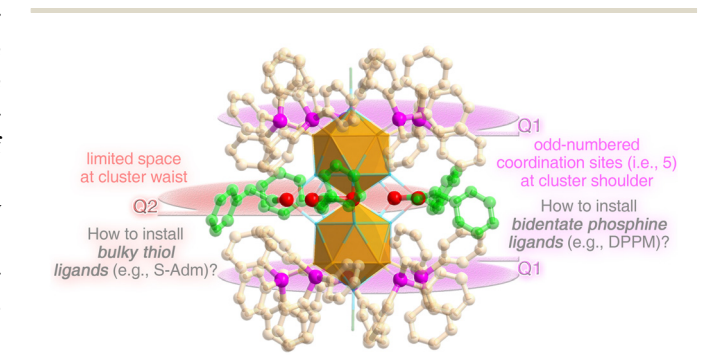
The rod-shaped Au₁₃Ag₁₂-S nanocluster follows a biicosahedral configuration via sharing a vertex Au atom between two Au₇Ag₆ nanobuilding blocks. 48 The Au atoms at the nanocluster shoulder are capped by monodentate PPh3 ligands, and the Ag atoms at the nanocluster waist are stabilized by SC2H4Ph ligands. Two longstanding questions remain unsolved for this nanocluster template (Scheme 1).

- (i) Altering monodentate PPh3 into bidentate phosphine ligands at the nanocluster shoulder (Scheme 1, Q1): five PPh₃ ligands are anchored onto each cluster shoulder via Au-P interactions, which puts forward a contradiction between the odd-numbered coordination sites (i.e., 5) and the evennumbered coordination ability (i.e., 2n) of the bidentate phosphines (e.g., DPPM).
- (ii) Arranging bulky thiol ligands into the limited space at the nanocluster waist (Scheme 1, Q2): five -SC₂H₄Ph ligands are arranged at the waist of Au₁₃Ag₁₂-S via Ag-S-Ag interactions. The waist space of the nanocluster is limited by considering the steric hindrance of the M25 metallic kernel from the inside out as well as the hindrance of the phosphine ligands from both sides to the middle. Accordingly, the thiol ligands in reported biicosahedral M25 nanoclusters are almost accompanied by alkyl chains or benzene rings with relatively small steric resistances. However, it remains challenging to install bulky thiol ligands (e.g., -S-Adm) into this limited space.

Collectively, it is unclear how the nanocluster framework undergoes self-adaption in the presence of bidentate phosphine ligands or bulky thiol ligands, and a comprehensive understanding of these longstanding questions calls for a new nanocluster template established from the biicosahedral M₂₅ nanostructure.

Several efforts have been made to install bidentate DPPM or bulky S-Adm ligands onto the M_{25} nanocluster surface (Scheme 2). The rod-shaped Au₁₃Ag₁₂-S nanocluster was synthesized by directly reducing the Au-Ag-Cl-PPh3-SC2H4Ph complexes with NaBH₄ (Scheme 2A). A set of control experiments were performed (Scheme 2B-D).

(i) The single thiol ligand control (Scheme 2B): the SC₂H₄Ph was substituted by the bulky S-Adm ligand, while the other experimental conditions remained unchanged. The Au₁₃Ag₁₂-Cl



Scheme 1 Schematic illustration of two long-lasting questions towards the rod-like biicosahedral M25 cluster template. (Q1) The substitution of monodentate PPh3 with bidentate phosphine ligands at the nanocluster shoulder. (Q2) The arrangement of bulky thiol ligands into the limited space at the nanocluster waist. The $[Au_{13}Ag_{12}(SC_2H_4Ph)_5(PPh_3)_{10}Cl_2]^{2+}$ nanocluster was exploited as the nanocluster model. Color labels: orange sphere, Au; light blue sphere, Ag; green sphere, Cl; red sphere, S; magenta sphere, P; pale pink sphere, C on PPh3 ligands; pale green sphere, C on SC₂H₄Ph ligands. For clarity, all H atoms are omitted.

vertical superposition

Nanoscale Horizons

vertical superposition

(A) Au Gl Ag (D) A

Scheme 2 Efforts for installing bidentate DPPM and bulky S-Adm ligands onto the biicosahedral nanocluster surface. (A) The preparation of the Au₁₃Ag₁₂-S nanocluster. (B) The preparation of the Au₁₃Ag₁₂-Cl nanocluster. (C) The preparation of the Au₁₃-DPPM nanocluster. (D) The preparation of the Au₁₉Ag₁₂ nanocluster. Color labels: orange sphere, Au; light blue sphere, Ag; green sphere, Cl; red sphere, S; magenta sphere, P; grey sphere, C; white sphere, H.

vertical superposition

nanocluster was obtained without surface thiol ligands. ⁴⁹ The $Au_{13}Ag_{12}$ -Cl nanocluster followed a similar configuration to $Au_{13}Ag_{12}$ -S with the only difference of waist stabilizers. For $Au_{13}Ag_{12}$ -Cl, six chlorine ligands stabilized the biicosahedral configuration via Ag–Cl–Ag interactions, playing the same role as SC_2H_4Ph ligands in $Au_{13}Ag_{12}$ -S. In other words, compared with SC_2H_4Ph , the bulky thiol ligand was challenging to be installed at the nanocluster waist, which was probably due to the large steric hindrance of S-Adm relative to the limited space.

(ii) The single phosphine ligand control (Scheme 2C): the substitution of PPh₃ with DPPM yielded a homogold $[Au_{13}(DPPM)_6]^{3+}$ (Au_{13} -DPPM for short) nanocluster. Accordingly, the biicosahedral configuration of M_{25} was broken to give rise to a mono-icosahedral nanocluster. The twelve surface Au atoms of the Au_{13} -DPPM nanocluster were capped by six DPPM ligands with an Au-DPPM-Au bonding mode. The obtained Au_{13} -DPPM nanocluster was the same as the previously reported one that was prepared via a thiol addition-induced synthetic procedure. Of note, the Ag component was absent in the final Au_{13} -DPPM. Such an absence might result from the instability of the possible $Ag_xAu_{13-x}(DPPM)_6$ products that only the homogold Au_{13} -DPPM nanocluster survived.

(iii) The dual thiol and phosphine ligand control (Scheme 2D): the PPh₃ and SC_2H_4Ph were substituted by bidentate DPPM and bulky S-Adm ligands simultaneously, which produced an $Au_{19}Ag_{12}$ nanocluster. The $Au_{19}Ag_{12}$ contained an M_{25} biicosahedron that was co-stabilized by Cl, DPPM, and S-Adm ligands. The rod-shaped M_{25} kernel was maintained by

comparing the overall structure of $Au_{19}Ag_{12}$ to that of $Au_{13}Ag_{12}$ -S or $Au_{13}Ag_{12}$ -Cl, while the surface DPPM-Au-SAdm motif structures followed a horizontal expansion mode. Collectively, based on the horizontally expanded biicosahedral $Au_{19}Ag_{12}$ nanocluster, both bidentate phosphine and bulky thiol ligands were installed onto the surface of rod-shaped nanoclusters.

The ESI-MS results of the Au₁₉Ag₁₂ nanocluster showed two groups of mass signals around 2853 and 4297 Da, corresponding to $[Au_{31-x}Ag_x(S-Adm)_6(DPPM)_6Cl_7]^{3+}$ and $[Au_{31-x}Ag_x(S-Adm)_6(DPPM)_6Cl_7]^{3+}$ $Adm)_6(DPPM)_6Cl_7^{2+}$ (x = 10-14), respectively (Fig. S1, ESI†). The excellent agreement of the experimental and simulated isotope patterns illustrated that the measured formulas of the largest peaks within these two groups were [Au₁₉Ag₁₂(S-Adm)₆ $(DPPM)_6Cl_7^{3+}$ and $[Au_{19}Ag_{12}(S-Adm)_6(DPPM)_6Cl_7]^{2+}$ (Fig. S1, insets, ESI†). In addition, ESI-MS results demonstrated that several metal positions of the Au₁₉Ag₁₂ nanocluster framework were jointly occupied by Au/Ag, which was reminiscent of the composition of Au₁₃Ag₁₂-S.⁴⁸ By combining the ESI-MS results and the crystal data, such Au_{31-x}Ag_x(S-Adm)₆(DPPM)₆Cl₇ nanoclusters are called Au₁₉Ag₁₂ in this work (see Tables S5-S7, ESI,† for more details of the naming of the three alloy nanoclusters in this work). Besides, previous studies of M13based cluster aggregates demonstrated that each icosahedral unit tended to hold eight free valence electrons within the nanocluster framework.31 Accordingly, for the [Au₁₉Ag₁₂ (S-Adm)₆(DPPM)₆Cl₇]²⁺ mass signal, the nominal electron count of the Au₁₉Ag₁₂ nanocluster was determined as 16 (i.e., 31(Au + Ag) -6(S-Adm) - 7(Cl) - 2(charge) = 16e), ⁵¹ tallying with the two icosahedral units in the cluster framework. The presence of Communication Nanoscale Horizons

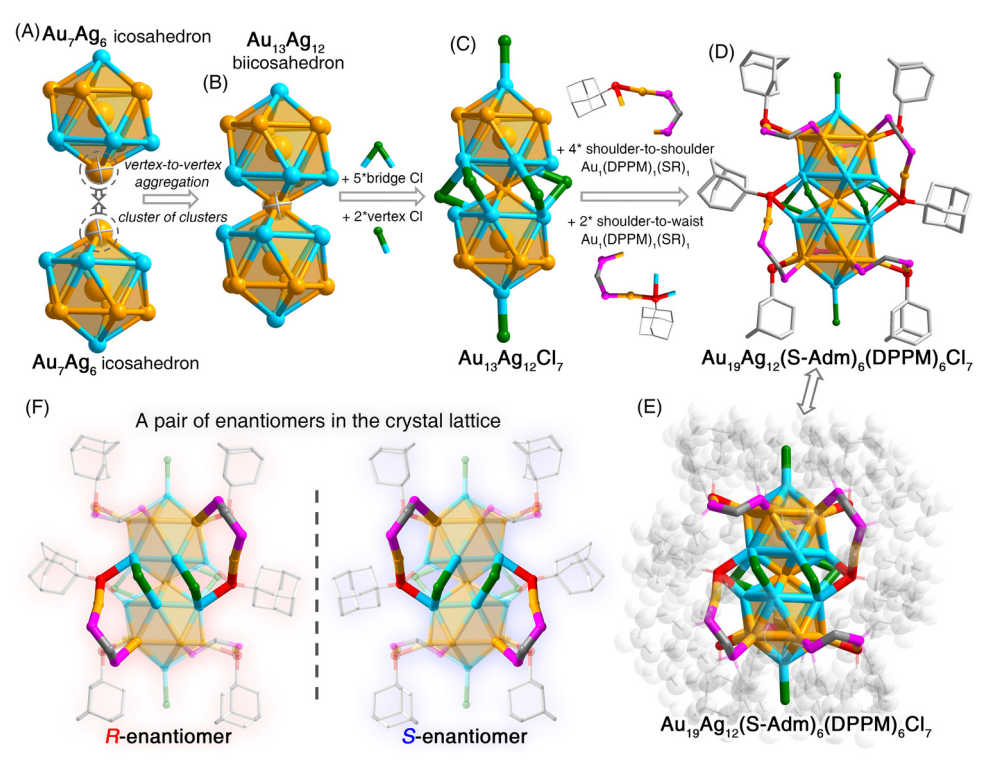


Fig. 1 Structural anatomy of the $Au_{19}Ag_{12}$ nanocluster. (A) The mono-icosahedral Au_7Ag_6 unit. (B) The biicosahedral Au_1Ag_1 2 kernel. (C) The $Au_{13}Ag_{12}Cl_7$ structure with two vertex Cl and five waist Cl ligands. (D) The $Au_{19}Ag_{12}(S-Adm)_6(DPPM)_6Cl_7$ with four shoulder-to-shoulder $Au_1(DPPM)_1(SR)_1$ and two shoulder-to-waist $Au_1(DPPM)_1(SR)_1$ surface motif structures. For clarity, the benzene rings on DPPM are omitted. (E) The overall structure of $Au_{19}Ag_{12}(S-Adm)_6(DPPM)_6Cl_7$. (F) A pair of nanocluster enantiomers in the crystal lattice. Color labels: orange sphere, Au; light blue sphere, Ag; green sphere, Cl; red sphere, S; magenta sphere, P; grey sphere, C; white sphere, H.

 $[Au_{31-x}Ag_x(S-Adm)_6(DPPM)_6Cl_7]^{3+}$ signals originated from the loss of an electron from the nanocluster molecule, which has also been observed previously in $Ag_{44}(SR)_{30}$ and $Pt_1Ag_{31}(SR)_{16}$ $(DPPM)_3Cl_3$ nanoclusters. 52,53

The structural anatomy of the $Au_{19}Ag_{12}$ nanocluster is shown in Fig. 1 and Fig. S2 (ESI†). First, two Au₇Ag₆ icosahedral nanobuilding blocks were assembled via sharing the vertex Au atom, giving rise to an Au13Ag12 biicosahedral kernel (Fig. 1A and B). Then, seven chlorine ligands, including five bridge Cl ligands at the waist and two Cl ligands at the vertex, were bonded onto the Au₁₃Ag₁₂ biicosahedron to yield an Au₁₃Ag₁₂Cl₇ structure (Fig. 1C). Finally, the Au₁₃Ag₁₂Cl₇ structure was enwrapped by six Au₁(DPPM)₁(S-Adm)₁ surface motif units to generate the overall structure of $Au_{19}Ag_{12}$ (Fig. 1D and E). Among these DPPM-Au-SAdm surface motifs, four were anchored onto the nanocluster with a shoulder-to-shoulder pattern, while the other two followed a shoulder to waist pattern. As shown in Fig. 1D and E, all bidentate DPPM ligands dually bound with a shoulder Au atom and a motif Au atom, while the bulky S-Adm ligands connected a shoulder Au atom and a motif Au atom (for motifs with a shoulder-to-shoulder pattern) or two waist Ag atoms and a motif Au atom (for motifs with a shoulder-to-waist pattern).

Two nanocluster enantiomers of the Au₁₉Ag₁₂ nanocluster were observed in the crystal lattice (Fig. 1F and Fig. S3, ESI†). Fig. 1F shows the mirrored structures of *R*-nanocluster and

S-nanocluster enantiomers. Furthermore, the crystallographic packing of these enantiomers followed a "lamellar eutectic" pattern, and the interlayer distance was determined as 28.897 Å from the (100) plane (Fig. S3, ESI†). Such a crystallographic packing pattern has been observed in several other crystal lattices consisting of nanocluster enantiomers. 54,55

Structurally, both Au₁₃Ag₁₂-S and Au₁₃Ag₁₂-Cl nanoclusters follow a "cluster of clusters" evolution mode and are assembled through the vertical superposition of icosahedral nanobuilding blocks. By comparison, the Au₁₉Ag₁₂ nanocluster is constructed by horizontally expanding the rod-like biicosahedral M25 cluster framework with several denotative Au₁(DPPM)₁(S-Adm)₁ motif structures (Fig. 2). A combination of Au₁₃Ag₁₂-S, Au₁₃Ag₁₂-Cl, and Au₁₉Ag₁₂ nanoclusters forms a platform for investigating the ligand effect in vertically and horizontally extending the M_{25} framework (Fig. 2). It is suggested that the biicosahedral M₂₅ framework is robust enough to load five thiol ligands or six chlorine ligands into the limited space at the nanocluster waist, yielding the Au₁₃Ag₁₂-S or Au₁₃Ag₁₂-Cl, respectively. Besides, although the bulky S-Adm ligands cannot be included into the limited space of the M25 framework, the further introduction of DPPM ligands triggers the self-adaption of the M25 framework. As a result, six couples of DPPM and S-Adm ligands are anchored onto the framework surface by tying six Au atoms. For the assembly between two M₁₃ icosahedra, because of the pulling effect of surface Au₁(DPPM)₁

Nanoscale Horizons Communication

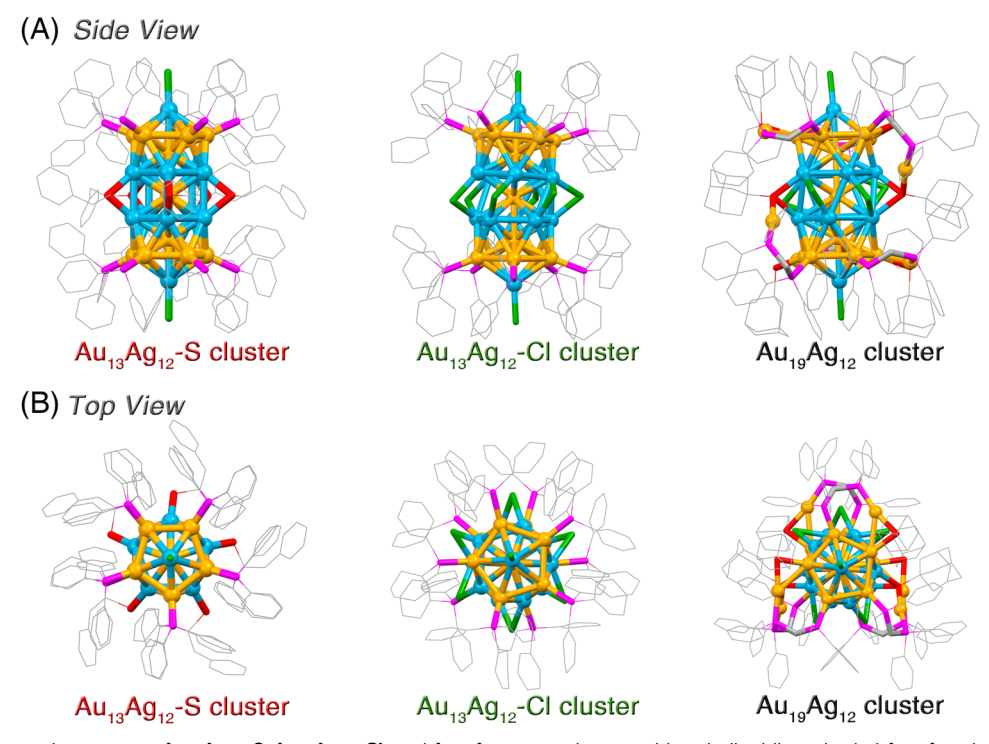


Fig. 2 Structural comparison among Au₁₃Ag₁₂-S, Au₁₃Ag₁₂-Cl, and Au₁₉Ag₁₂ nanoclusters with a similar biicosahedral Au₁₃Ag₁₂ kernel. (A) Side views of Au₁₃Ag₁₂-S, Au₁₃Ag₁₂-Cl, and Au₁₉Ag₁₂ nanoclusters. (B) Top views of Au₁₃Ag₁₂-S, Au₁₃Ag₁₂-Cl, and Au₁₉Ag₁₂ nanoclusters. Color labels: orange sphere, Au; light blue sphere, Ag; green sphere, Cl; red sphere, S; magenta sphere, P; grey sphere, C. For clarity, all H atoms are omitted.

(S-Adm)₁ motif structures, the distortion degree of icosahedral Au₇Ag₆ nanobuilding blocks in Au₁₉Ag₁₂ is higher than that in $Au_{13}Ag_{12}$ -S or $Au_{13}Ag_{12}$ -Cl.

The comparison of the corresponding bond lengths is depicted in Fig. S4 (ESI†). Specifically, the bond length distributions of these M₁₃-assembled nanoclusters (i.e., Au₁₃Ag₁₂-S, Au₁₃Ag₁₂-Cl, and Au₁₉Ag₁₂) are similar in terms of the Au(kernel)-M(icosahedral surface), M(icosahedral surface)-M(icosahedral surface), Ag(icosahedral surface)-Cl(vertex), and Au(icosahedral surface)-P(shoulder) bonds (M = Au/Ag; Fig. S4A-D, ESI†), which results from the robust assembly between two icosahedral subunits. The Ag(icosahedral surface)-Cl(waist) bond lengths of Au₁₉Ag₁₂ are much longer than those of Au₁₃Ag₁₂-Cl, and such an elongation originates from the more twisted assembly between two icosahedral Au₇Ag₆ subunits in Au₁₉Ag₁₂ (Fig. S4E, ESI†). The most significant difference in bond length lies in the Ag(icosahedral surface)-S(waist) interactions between Au₁₉Ag₁₂ and Au₁₃Ag₁₂-S nanoclusters, where the average Ag(icosahedral surface)-S(waist) bond length in Au₁₉Ag₁₂ is 2.515 Å, much longer than that of Au₁₃Ag₁₂-S (2.432 Å; Fig. S4F, ESI†). Such a difference is rational, given that the S-Adm ligand in Au₁₉Ag₁₂ is bulkier than SC₂H₄Ph in Au₁₃Ag₁₂-S, resulting in extended metal-thiol interactions in Au₁₉Ag₁₂ so that the bulky S-Adm ligands can be installed into the limited space at the cluster waist.

Because of their different molecular configurations and intercluster interactions, these four M₁₃-based nanoclusters exhibit disparate crystal packing modes (Fig. S5, ESI†). The ligand-directed intercluster packings of these M13-based

nanoclusters were then compared. Specifically, both Au₁₃Ag₁₂-S and $Au_{13}Ag_{12}$ -Cl nanoclusters contain C-H··· π and H···Cl interactions, while there are only $C-H\cdots\pi$ interactions in the crystal structure of Au₁₃-DPPM. For the Au₁₉Ag₁₂ nanocluster, several types of intercluster interactions are detected, including C-H $\cdots \pi$, $H \cdot \cdot \cdot Cl$, and $\pi \cdot \cdot \cdot \pi$ interactions (Fig. S5, ESI†).

The optical absorptions of these icosahedron-based nanoclusters were then compared. The CH₂Cl₂ solution of the Au₁₉Ag₁₂ nanocluster showed three distinct absorptions at 455, 515, and 710 nm and two shoulder bands at 415 and 535 nm (Fig. S6, ESI†). By comparison, the UV-vis spectrum of the Au₁₃Ag₁₂-S nanocluster displayed three absorptions at 425, 480, and 650 nm, while those of the Au₁₃Ag₁₂-Cl nanocluster were centered at 420, 510, and 645 nm. The mono-icosahedral Au₁₃-DPPM nanocluster exhibited an intense band at 440 nm and a shoulder band around 800 nm (Fig. S7, ESI†). Such differences in optical absorptions of these icosahedron-based nanoclusters originated from their distinct electronic structures. Yuan et al. have unveiled the strong electron coupling between substituent icosahedral units based on the monoicosahedral Ag13 and tetra-icosahedral Ag61 nanoclusters, which resulted in the red-shift of their main absorptions.⁴⁰ In this work, the red-shifted absorption was also observed by comparing the intense optical bands of bi-icosahedral $Au_{19}Ag_{12}$, $Au_{13}Ag_{12}$ -S, and $Au_{13}Ag_{12}$ -Cl nanoclusters (710, 650, and 645 nm, respectively) with the main absorption of the mono-icosahedral Au₁₃-DPPM nanocluster (440 nm), which might also arise from the electron coupling between the substituent icosahedral subunits. Of note, for the Au13-DPPM

Communication Nanoscale Horizons

nanocluster, its 440 nm absorption was regarded as the main absorption of the icosahedral kernel since the M_{13} -based absorptions (or electronic transitions) were always located in nearby areas. ^{56–58} In addition, owing to the complete protection of the $Au_{13}Ag_{12}$ biicosahedral kernel by bridging Cl and surface $Au_1(DPPM)_1(SR)_1$ structures, the $Au_{19}Ag_{12}$ nanocluster was highly stable and could maintain its composition and configuration within 20 days, derived from its unchanged optical absorptions over time (Fig. S8, ESI†).

The photoluminescent properties of these four nanoclusters were then compared. As shown in Fig. S9, ESI† the monoicosahedral Au_{13} -DPPM was non-emissive, while the other three biicosahedral nanoclusters were emissive. Specifically, the PL intensity of these emissive nanoclusters followed a sequence of $Au_{13}Ag_{12}$ -S > $Au_{13}Ag_{12}$ -Cl > $Au_{19}Ag_{12}$. As for the emissive wavelength, the $Au_{19}Ag_{12}$, $Au_{13}Ag_{12}$ -S, and $Au_{13}Ag_{12}$ -Cl nanoclusters emitted at 825, 735, and 765 nm, respectively. In this context, the emission wavelength of $Au_{19}Ag_{12}$ occurred in the NIR-I region and exhibited a significant red-shift relative to those of $Au_{13}Ag_{12}$ -S and $Au_{13}Ag_{12}$ -Cl (Fig. S9, ESI†).

3. Conclusions

In summary, the horizontal expansion of the rod-like biicosahedral M₂₅ cluster framework was accomplished, yielding an $\left[Au_{19}Ag_{12}(S\text{-}Adm)_{6}(DPPM)_{6}Cl_{7}\right] ^{2+}$ nanocluster. The structural determination resolved two decades-long questions towards rod-shaped multi-icosahedral nanoclusters, including (i) how to install bidentate phosphine ligands onto the nanocluster shoulder and (ii) how to load bulky thiol ligands into the limited space of the nanocluster waist? A combination of the new [Au₁₉Ag₁₂(S-Adm)₆(DPPM)₆Cl₇]²⁺ nanocluster in this work and previously reported $[Au_{13}Ag_{12}(PPh_3)_{10}Cl_8]^{2+}$ or $[Au_{13}Ag_{12}(SR)_5]$ (PPh₃)₁₀Cl₂]²⁺ constituted a platform for mapping out the ligand effect in vertically/horizontally expanding icosahedral M₁₃-based nanoclusters. Overall, this work presents the horizontal expansion of rod-shaped nanoclusters, which broadens the research towards the "cluster of clusters" and hopefully inspires more work on constructing M₁₃-based aggregates from vertically and horizontally growing extensions.

Data availability

All the data supporting this article have been included in the main text and the ESI. $\!\!\!\!\!\!^{\dagger}$

Author contributions

C. Z. and P. P. carried out the experiments and analyzed the data. X. W., Z. L. and C. C. assisted the analysis. X. K. and M. Z. designed the project, analyzed the data, and wrote the manuscript.

Conflicts of interest

There are no conflicts to declare.

Acknowledgements

We acknowledge the financial support provided by the National Natural Science Foundation of China (21631001, 21871001, and 22101001), the Ministry of Education, and the University Synergy Innovation Program of Anhui Province (GXXT-2020-053).

References

- 1 R. Jin, C. Zeng, M. Zhou and Y. Chen, *Chem. Rev.*, 2016, **116**, 10346–10413.
- 2 I. Chakraborty and T. Pradeep, Chem. Rev., 2017, 117, 8208-8271.
- 3 X. Kang, Y. Li, M. Zhu and R. Jin, *Chem. Soc. Rev.*, 2020, **49**, 6443–6514.
- 4 S. Sharma, K. Chakrahari, J. Saillard and C. W. Liu, Acc. Chem. Res., 2018, 51, 2475–2483.
- 5 T. Kawawaki, Y. Kataoka, M. Hirata, Y. Iwamatsu, S. Hossain and Y. Negishi, *Nanoscale Horiz.*, 2021, **6**, 409–448.
- 6 Y. Jin, C. Zhang, X. Dong, S. Zang and T. C. W. Mak, *Chem. Soc. Rev.*, 2021, 50, 2297–2319.
- 7 J. Yan, B. K. Teo and N. Zheng, Acc. Chem. Res., 2018, 51, 3084–3093.
- 8 X. Kang and M. Zhu, Chem. Soc. Rev., 2019, 48, 2422-2457.
- 9 A. W. Cook and T. W. Hayton, *Acc. Chem. Res.*, 2018, **51**, 2456–2464.
- 10 N. Xia and Z. Wu, Chem. Sci., 2021, 12, 2368-2380.
- 11 S. Kenzler and A. Schnepf, Chem. Sci., 2021, 12, 3116-3129.
- 12 G. Salassa and T. Bürgi, Nanoscale Horiz., 2018, 3, 457-463.
- 13 M. Agrachev, M. Ruzzi, A. Venzo and F. Maran, Acc. Chem. Res., 2019, 52, 44–52.
- 14 K. Kwak and D. Lee, Acc. Chem. Res., 2019, 52, 12-22.
- 15 B. Nieto-Ortega and T. Bürgi, *Acc. Chem. Res.*, 2018, **51**, 2811–2819.
- 16 M. Hesari, H. Ma and Z. Ding, *Chem. Sci.*, 2021, **12**, 14540–14545.
- 17 X.-Q. Liang, Y.-Z. Li, Z. Wang, S.-S. Zhang, Y.-C. Liu, Z.-Z. Cao, L. Feng, Z.-Y. Gao, Q.-W. Xue, C.-H. Tung and D. Sun, *Nat. Commun.*, 2021, 12, 4966.
- 18 E. Ubasart, I. M. Marin, J. M. Asensio, G. Mencia, Á. López-Vinasco, C. García-Simón, I. Rosal, R. Poteau, B. Chaudret and X. Ribas, *Nanoscale Horiz.*, 2022, 7, 607–615.
- 19 S. Li, X.-Y. Dong, K.-S. Qi, S.-Q. Zang and T. C. W. Mak, J. Am. Chem. Soc., 2021, 143, 20574–20578.
- 20 R. W. Y. Man, H. Yi, S. Malola, S. Takano, T. Tsukuda, H. Häkkinen, M. Nambo and C. M. Crudden, *J. Am. Chem. Soc.*, 2022, 144, 2056–2061.
- 21 T. Kawawaki, Y. Kataoka, M. Hirata, Y. Akinaga, R. Takahata, K. Wakamatsu, Y. Fujiki, M. Kataoka, S. Kikkawa, A. S. Alotabi, S. Hossain, D. J. Osborn, T. Teranishi,

G. G. Andersson, G. F. Metha, S. Yamazoe and Y. Negishi,

Nanoscale Horizons

22 Z.-J. Guan, R.-L. He, S.-F. Yuan, J.-J. Li, F. Hu, C.-Y. Liu and Q.-M. Wang, Angew. Chem., Int. Ed., 2022, 61, e202116965.

Angew. Chem., Int. Ed., 2021, 60, 21340-21350.

- 23 H. Yi, S. M. Han, S. Song, M. Kim, E. Sim and D. Lee, Angew. Chem., Int. Ed., 2021, 60, 22293-22300.
- 24 G. Deng, B. K. Teo and N. Zheng, J. Am. Chem. Soc., 2021, 143, 10214-10220.
- 25 G.-T. Xu, X.-Y. Chang, K.-H. Low, L.-L. Wu, Q. Wan, H.-X. Shu, W.-P. To, J.-S. Huang and C.-M. Che, Angew. Chem., Int. Ed., 2022, 61, e202200748.
- 26 G. Li, X. Sui, X. Cai, W. Hu, X. Liu, M. Chen and Y. Zhu, Angew. Chem., Int. Ed., 2021, 60, 10573-10576.
- 27 S. Lee, M. S. Bootharaju, G. Deng, S. Malola, H. Häkkinen, N. Zheng and T. Hyeon, J. Am. Chem. Soc., 2021, 143, 12100-12107.
- 28 X. Kang, X. Wei, S. Jin, Q. Yuan, X. Luan, Y. Pei, S. Wang, M. Zhu and R. Jin, Proc. Natl. Acad. Sci. U.S.A., 2019, 116, 18834-18840.
- 29 M. Qu, H. Li, L.-H. Xie, S.-T. Yan, J.-R. Li, J.-H. Wang, C.-Y. Wei, Y.-W. Wu and X.-M. Zhang, J. Am. Chem. Soc., 2017, 139, 12346-12349.
- 30 N. A. Sakthivel and A. Dass, Acc. Chem. Res., 2018, 51, 1774-1783.
- 31 X. Kang and M. Zhu, Coord. Chem. Rev., 2019, 394, 1-38.
- 32 B. K. Teo and H. Zhang, Coord. Chem. Rev., 1995, 143, 611-636.
- 33 B. K. Teo and H. Zhang, Inorg. Chim. Acta, 1988, 144, 173-176.
- 34 B. K. Teo and H. Zhang, *Polyhedron*, 1990, **9**, 1985–1999.
- 35 B. K. Teo and H. Zhang, J. Cluster Sci., 1990, 2, 223-228.
- 36 Y. Shichibu, Y. Negishi, T. Watanabe, N. K. Chaki, H. Kawaguchi and T. Tsukuda, J. Phys. Chem. C, 2007, 111, 7845-7847.
- 37 M. S. Bootharaju, S. M. Kozlov, Z. Cao, M. Harb, N. Maity, A. Shkurenko, M. R. Parida, M. N. Hedhili, M. Eddaoudi, O. F. Mohammed, O. M. Bakr, L. Cavallo and J. Basset, J. Am. Chem. Soc., 2017, 139, 1053-1056.
- 38 R. Jin, C. Liu, S. Zhao, A. Das, H. Xing, C. Gayathri, Y. Xing, N. L. Rosi, R. R. Gil and R. Jin, ACS Nano, 2015, 9,
- 39 T.-H. Chiu, J.-H. Liao, F. Gam, I. Chantrenne, S. Kahlal, J.-Y. Saillard and C. W. Liu, J. Am. Chem. Soc., 2019, 141, 12957-12961.
- 40 S. Yuan, C. Xu, W. Liu, J. Zhang, J. Li and Q. Wang, J. Am. Chem. Soc., 2021, 143, 12261-12267.

- 41 S. Yang, J. Chai, T. Chen, B. Rao, Y. Pan, H. Yu and M. Zhu, Inorg. Chem., 2017, 56, 1771-1774.
- 42 S. Yang, J. Chai, Y. Lv, T. Chen, S. Wang, H. Yu and M. Zhu, Chem. Commun., 2018, 54, 12077-12080.
- 43 Y. Song, F. Fu, J. Zhang, J. Chai, X. Kang, P. Li, S. Li, H. Zhou and M. Zhu, Angew. Chem., Int. Ed., 2015, 54, 8430-8434.
- 44 H. Qian, W. T. Eckenhoff, Y. Zhu, T. Pintauer and R. Jin, J. Am. Chem. Soc., 2010, 132, 8280-8281.
- 45 L. Xu, Q. Li, T. Li, J. Chai, S. Yang and M. Zhu, Inorg. Chem. Front., 2021, 8, 4820-4827.
- 46 S. Jin, M. Zhou, X. Kang, X. Li, W. Du, X. Wei, S. Chen, S. Wang and M. Zhu, Angew. Chem., Int. Ed., 2020, 59, 3891-3895.
- 47 F. Hu, Z. Guan, G. Yang, J. Wang, J. Li, S. Yuan, G. Liang and Q. Wang, J. Am. Chem. Soc., 2021, 143, 17059-17067.
- 48 S. Wang, X. Meng, A. Das, T. Li, Y. Song, T. Cao, X. Zhu, M. Zhu and R. Jin, Angew. Chem., Int. Ed., 2014, 53, 2376-2380.
- 49 B. K. Teo and H. Zhang, Angew. Chem., Int. Ed. Engl., 1992, 104, 445-447.
- 50 S. Jin, W. Du, S. Wang, X. Kang, M. Chen, D. Hu, S. Chen, X. Zou, G. Sun and M. Zhu, Inorg. Chem., 2017, 56, 11151-11159.
- 51 M. Walter, J. Akola, O. Lopez-Acevedo, P. D. Jadzinsky, G. Calero, C. J. Ackerson, R. L. Whetten, H. Grönbeck and H. Häkkinen, Proc. Natl. Acad. Sci. U.S.A., 2008, 105, 9157-9162.
- 52 A. Desireddy, B. E. Conn, J. Guo, B. Yoon, R. N. Barnett, B. M. Monahan, K. Kirschbaum, W. P. Griffith, R. L. Whetten, U. Landman and T. P. Bigioni, Nature, 2013, 501, 399-402.
- 53 X. Kang, S. Jin, L. Xiong, X. Wei, M. Zhou, C. Qin, Y. Pei, S. Wang and M. Zhu, Chem. Sci., 2020, 11, 1691-1697.
- 54 X. Kang, F. Xu, X. Wei, S. Wang and M. Zhu, *Sci. Adv.*, 2019, 5, eaax7863.
- 55 C. Xu, Q. Yuan, X. Wei, H. Li, H. Shen, X. Kang and M. Zhu, Chem. Sci., 2022, 13, 1382-1389.
- 56 M. Zhu, C. M. Aikens, F. J. Hollander, G. C. Schatz and R. Jin, J. Am. Chem. Soc., 2008, 130, 5883-5885.
- 57 K. L. D. M. Weerawardene, P. Pandeya, M. Zhou, Y. Chen, R. Jin and C. M. Aikens, J. Am. Chem. Soc., 2009, 141, 18715-18726.
- 58 J. Kong, W. Zhang, Y. Wu and M. Zhou, Aggregate, 2022, DOI: 10.1002/agt2.207.